Magnetism in complex atomic structures: Grain boundaries in nickel

Barbara Szpunar, Uwe Erb, and Gino Palumbo
Department of Materials and Metallurgical Engineering, Queen's University, Kingston, Ontario, Canada K7L 3N6

K. T. Aust
Department of Metallurgy and Materials Science, University of Toronto, Toronto, Ontario, Canada M5S 1A4

Laurent J. Lewis
Département de Physique et Groupe de Recherche en Physique et Technologie des Couches Minces (GCM), Université de Montréal, Case postale 6128, Succursale Centre-Ville, Montréal, Québec, Canada H3C 3J7

(Received 20 July 1995)

We study the influence of structural disorder on the magnetic properties of nanocrystalline nickel, in particular the $\Sigma 13$ and $\Sigma 5$ special grain boundaries and the extreme case of a purely amorphous sample, for which experimental results are controversial. The configurations were minimized using molecular-dynamics simulations with embedded-atom method potentials. The electronic-structure calculations are performed using the tight-binding linear muffin-tin orbital atomic-sphere-approximation approach. Our calculations reveal that the magnetic moment is rather insensitive to the amount of disorder present in the structure, varying by at most 20% at the special grain boundaries. These results correlate extremely well with recent observations in electroplated nickel that the magnetic moment depends very little on grain size, down to about 10 nm, i.e., is not critically determined by the amount of matter in the grain boundaries. Even in the limit where all the volume belongs to interfaces and is amorphous, the average magnetic moment is reduced by only about 15%. The local moments in amorphous nickel vary between $0.4\mu_B$ and $0.6\mu_B$, and a weak correlation between the magnitude of the local moment and the average nearest-neighbor distance is observed.

I. INTRODUCTION

In recent years, enormous experimental progress has been made in the development of new magnetic materials. However, up to now, most of the theoretical calculations have neglected the details of the real atomic structure of materials—and in particular the effect of defects such as grain boundaries—on the magnetic properties. These ''local'' contributions are most probably negligible in materials with large grains, since the volume of a grain boundary is only a small fraction of the total volume, but in the recently developed nanocrystalline materials, the percentage of atoms at grain boundaries can be as high as 50%.[1,2] For these materials, the effect of structural disorder at interfaces can no longer be neglected. In the present work, we will describe the effect of the structural disorder at grain boundaries on the local magnetic moment, and concurrently calculate the magnetic properties of the amorphous phase in nickel. These results will then be used to assess the magnetic properties of nanocrystalline nickel.

Nanocrystalline materials are among the most intriguing new developments in the field of materials synthesis. Structurally, these materials can be classified as a transitional state between normal crystalline and amorphous materials. However, their properties are quite unique and not intermediate to their amorphous or normal crystalline counterparts. Over the past 15 years, these properties have stimulated considerable interest in the areas of production, characterization and potential applications. Numerous synthesis techniques have been developed including inert gas condensation, sol-gel processing, reactive sputtering, electroplating, etc.[1]

The magnetic properties of any polycrystalline ferromagnetic material strongly depend on microstructural parameters such as crystallographic texture, internal stress, grain shape anisotropy, grain size distribution, etc.[3,4] For nanocrystalline materials in which the grain size approaches the dimensions of the domain wall thickness, considerable changes in the magnetic behavior are expected. For example, it has been shown that the grain size in devitrified amorphous $Fe_{73.5}Si_{13.5}B_9Nb_3Cu$ alloys has a strong effect on the soft magnetic behavior.[5–7] In these materials, the size of α–Fe-Si grains (of the order of 10 nm) is controlled in the nanocrystalline range by Cu and Nb additions, which act as nucleation agent and grain growth inhibitor, respectively. The best soft magnetic properties were observed for grain sizes below 20 nm.[7] Similar results were reported for Fe-Zr-B alloys with grain sizes in the 10–20 nm range.[8]

In a recent review, Gleiter[1] reported a reduction in the saturation magnetization by 40% for iron with 6 nm grain size compared to only 2% for metallic iron glasses. It was proposed[1] that the magnetic microstructure of nanocrystalline iron differs from that of conventional polycrystalline iron in that every crystallite is a single ferromagnetic domain. More recently, Wagner *et al.*[9] studied the magnetic microstructure of nanocrystalline iron (7 nm grain size) by small angle neutron scattering. They proposed that the material consists of ferromagnetic grains separated by a nonmagnetic or weakly magnetic interface component with a density of about 40% of that of the crystallites. Furthermore, they concluded that, even in the absence of an external magnetic field, the magnetic correlations are not confined to individual crystallites but extend across the interface and therefore af-

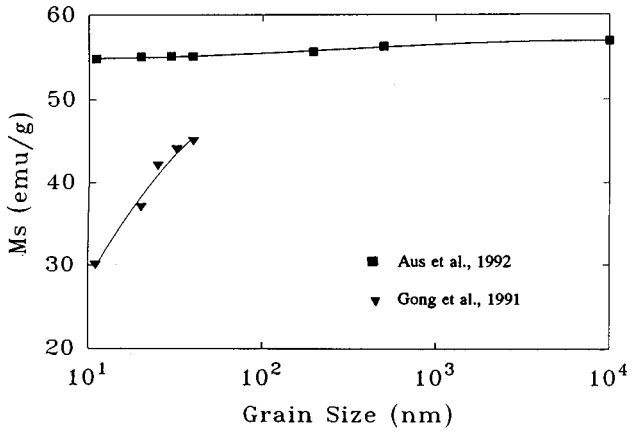

FIG. 1. Saturation magnetization of Ni as a function of grain size (from Ref. 16).

fect the magnetization of several hundred grains.

A transition from multidomain to single domain grains has been proposed to be responsible for the maximum coercivity observed in Co-W alloys for grain sizes in the 10–40 nm range.[10] Strong effects of particle size on saturation magnetization and coercivity have also been observed in the study of ultrafine particles.[11–13] For example, for ultrafine particles (50–10 nm) of Ni, Co, and Fe, Gong *et al.*[12] reported maxima in coercivity which, according to their calculations, correspond to a critical particle size at which the transition to single-domain particles occurs. The decrease in coercivity below the critical size was attributed to the ferromagnetic to superparamagnetic transition. A similar transition to superparamagnetic behavior for ultrafine Fe and Ni particles (5–20 nm range) was also reported by Gangopadhyay *et al.*[11]

Further, particle size dependence of magnetic behavior is observed in ultrafine granular films[14] or nanocomposites[15] where small ferroelectric particles are embedded in nonmagnetic matrices such as SiO_2. Transitions from ferromagnetic to superparamagnetic or paramagnetic behavior are typically found when the grain size of the isolated particles decreases below a certain value.

In contrast to the results reported for ultrafine particles,[11,13] we have recently shown that the saturation magnetization of nanocrystalline Ni produced by electroplating is not strongly dependent on grain size.[16] A decrease in grain size from conventional material (grain size ~ 100 μm) to nanocrystals (~ 10 nm) resulted in a reduction of the saturation magnetization by less than 10%. These results are shown in Fig. 1 which also contains the data reported by Gong *et al.*[12] for ultrafine Ni particles produced by inert gas condensation. The strong decrease in the saturation magnetization observed by Gong *et al.*[12] is probably due to the oxide layers which form on the individual crystallites of their Ni powder. In fully dense electroplated material, on the other hand, oxidation effects are negligible and, therefore, almost constant saturation magnetization is observed over the entire grain size range.

Mössbauer spectroscopy experiments on nanocrystalline iron[17] at low temperatures reveal the existence of two contributions to the total spectrum: from the nanocrystals themselves at small values of the hyperfine field, and from the interfaces for larger values of hyperfine field. While the interfacial component decreases rapidly with increasing temperature, becoming almost negligible at room temperature, the crystalline component is much less sensitive to temperature variations. This suggests a strong dependence of the magnetization saturation of nanocrystals as low temperatures are approached, in contradiction with the recent observation[18] that the saturation magnetization in nanocrystalline and crystalline nickel behave in essentially the same manner at the low temperature (albeit it is smaller in the latter than in the former).

There exist several theoretical calculations of the magnetic moments of pure amorphous transition metals. Earlier calculations[19] indicated that structural disorder tends to ''smear out'' the density of states, leading to a reduction of the density of states at the Fermi energy and a concomitant significant decrease of the local magnetic moment. More recent calculations[20] show, indeed, that the average moment of amorphous iron ($2.0\mu_B$) decreases due to an effective broadening of the bands in comparison to the bcc-crystalline phase (arising from a larger coordination in the amorphous state). The local moments are broadly distributed ($0.5\mu_B$ standard deviation) and the average moment depends strongly on the density. Other recent calculations[21] show that at low densities, the average moment in amorphous iron and cobalt is only slightly larger than for its crystalline counterpart, with a narrow distribution of the local moments around its mean value and equals correspondingly $2.3\mu_B$ and $1.64\mu_B$. First-principles calculations with self-consistency obtained for crystalline iron[22] lead, in the amorphous phase, to a large average moment ($2.46\mu_B$) with a wide distribution of local moments (between $1.5\mu_B$ and $4.0\mu_B$). In a very recent paper,[23] however, it has been found that, at the equilibrium density for bcc iron, the ferromagnetic state is *not* the state of lowest energy (average moment $2.4\mu_B$). For amorphous cobalt and nickel (at the density of the corresponding equilibrium crystal), in contrast, it is found that the ferromagnetic state is the state of lowest energy, and the average magnetic moment is larger than that of the crystal, namely $1.65\mu_B$ for cobalt and $0.64\mu_B$ for nickel, with a standard deviation of about $0.05\mu_B$. In those calculations,[23] however, the number of atoms in the supercell was small (16) and the same structural model was used to study the influence of chemical effects.

In view of such conflicting reports, we have initiated a detailed study of the effect of structural disorder introduced by grain boundaries and the amorphous state on the magnetic properties of nanocrystalline metals. In the following sections we will report some results of these calculations.

II. STRUCTURAL DISORDER IN NANOCRYSTALLINE MATERIALS

Over the past three decades, a central goal of research conducted in the field of grain boundaries in conventional polycrystalline materials has been to understand the relationship between grain boundary structure and physical properties. Today it is known that there are basically two types of grain boundaries in a material: random and special boundaries.[24] Kronberg and Wilson[25] indicated the impor-

tance of the concept of a coincidence site lattice (CSL), whereby, at certain crystallographic misorientations, a three-dimensional lattice could be constructed with lattice points common to both crystals. The CSL is thus considered the smallest common sublattice of the adjoining grains. The volume ratio of the unit cell of the CSL to that of the crystal is described by the parameter Σ which can also be considered the reciprocal density of coincident sites. All grain boundaries can be represented by an appropriate CSL description if Σ is allowed to approach infinite values.

Ranganathan[26] presented a general procedure for obtaining CSL relationships about general rotation axes. Although all grain boundaries can be represented by an exact CSL relationship, Σ may achieve very high values of questionable physical significance. Only boundaries which have low Σ values are usually considered special boundaries.

In nanocrystalline materials, the grain boundary density, and therefore the volume fraction of atoms located at grain boundary sites, can achieve very high values.[1] For example, for a grain size of 10 nm, about 30% of all atoms are at the boundary, assuming a grain boundary thickness of 1 nm.[2] Therefore, the properties of such materials are strongly controlled by the structural disorder introduced by grain boundaries.

In a previous publication,[27] we have examined the special high-angle grain boundary that introduces the least structural disorder, namely the $\Sigma 3$ boundary, whose structure can be generated by a series of stacking faults in the perfect crystal. As expected, the local moments do not vary much, ranging between 0.58 and $0.59\mu_B$ from site to site with the average value $0.59\mu_B$. We have also studied the $\Sigma 5$ grain boundary, generated by a 36.9° twist about [100] axis, where the sensitivity of the local moments on the structural disorder was found to be larger.[27] In order to obtain the relaxed structure of the $\Sigma 5$ grain boundary, the Monte Carlo method was used to minimize the total energy of the system, using the potential of Dagens[28] to represent the interactions between the atoms.

In the present work, we obtain the relaxed structure using the technique of molecular dynamics (MD). In the molecular-dynamics method,[29] the Newtonian equations of motion of an ensemble of particles interacting via some specified potential are solved numerically, so that not only the static quantities (like in Monte Carlo) but also the dynamic properties of the system can be studied. The ''technology'' of potentials has evolved rapidly in recent years and, in particular, the semiempirical embedded-atom-method (EAM) potentials[30] (which are based on the quantum-mechanical density-functional theory) have proved extremely successful in describing several properties of transition metals. In the present molecular-dynamics simulations of nickel, we use the EAM potential developed by Foiles, Baskes, and Daw.[31] We find that this approach leads, for the $\Sigma=5$ grain boundary at zero temperature, to results similar to those discussed in our previous paper,[27] using the Dagens potential and the zero-temperature Monte Carlo technique. In the present work, the structures (grain boundaries and amorphous state) were relaxed at nonzero temperature (100 K), so as to be able to escape from local minima. The MD simulations were performed under constant pressure, and the ''Nosé thermostat'' method[32] was used to control the temperature.

In order to study the effect of local structural disorder on the magnetic moment associated with various types of grain boundaries, the following approach was used. First, we examined special high-angle grain boundaries. In order to uncover trends in the magnetic properties, we studied grain boundaries with significantly different twist angles, namely the highly-symmetric $\Sigma 5$, a 36.9° twist about [100], and for comparison the $\Sigma 13$, a 22.6° twist about [100]. At the other end of the spectrum, we consider the general high-angle (''random'') grain boundary, which is more difficult to model because its structure is poorly understood. For the purpose of the present study, we assume that random grain boundaries are amorphous. It should be noted that random grain boundaries are generally not amorphous; the amorphous state, however, can be considered the worst possible case of structural disorder introduced by grain boundaries. Thus, the grain boundary structures that are present in real nanocrystalline materials can be expected to fall within the range which is limited by the best possible case—a $\Sigma 3$ boundary, which affects magnetic properties in a negligible way[27]—and the worst possible case of a simulated amorphous grain boundary.

III. RESULTS AND DISCUSSION

A. Measures of disorder

Before analyzing our MD results, we introduce several quantities which we will use to characterize disorder and which will provide a quantitative measure of the deviation of the disordered system from the ideal reference structure, here the fcc crystal at 0 K.

First we define two parameters characterizing local disorder: the local average distance, $d(i)_Z$, and the average absolute deviation from equilibrium, $\Delta d(i)_Z$. $d(i)_Z$ is defined, for a given site i, as the average distance between the site and its twelve $(=Z)$ nearest neighbors (appropriate to the fcc structure):

$$d(i)_Z=\frac{1}{12}\sum_{\mathrm{NN}} r_{ij}\,. \tag{3.1}$$

Expressing r_{ij} in terms of the fcc nearest-neighbor distance, then, evidently, $d(i)_Z$ is equal to one for all sites in the ideal fcc lattice. $\Delta d(i)_Z$ is defined as the average absolute deviation for the above twelve nearest-neighbor distances:

$$\Delta d(i)_Z=\frac{1}{12}\sum_{\mathrm{NN}} |r_{ij}-1|. \tag{3.2}$$

Thus $\Delta d(i)_Z$ is zero for the ideal fcc lattice. These two parameters provide information about local disorder; we will use these, in the course of our discussion, to establish correlations between local disorder and local magnetic moments.

We also introduce a parameter $\Lambda(r)$ to provide a ''global'' measure of disorder within a sphere of radius r. As is well known, disorder in amorphous material depends on the length scale. At short distances, some order is usually present (because of hard-sphere exclusion, for instance), which is lost at large distances. Thus an amorphous material is characterized by the presence of short-range order and the absence of long-range order. This is apparent, in particular, in

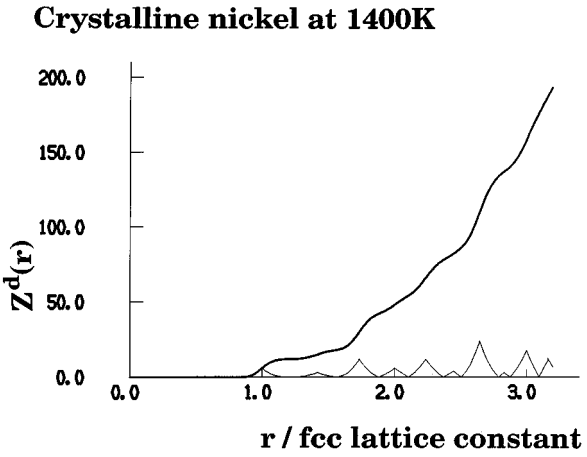

FIG. 2. Integrated radial distribution function for nickel at 1400 K.

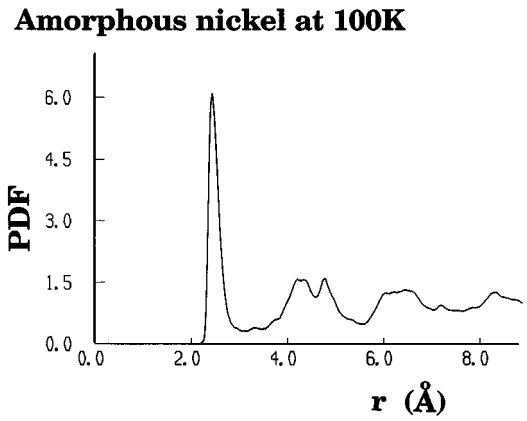

FIG. 3. Pair distribution function for the present model of amorphous nickel.

the radial distribution function, $\rho(r)$, which shows structure at short distances, and becomes flat at large distances. We define $\Lambda(r)$ as the average, over all atoms, of the absolute deviation of the radial position of atoms from their corresponding position in the reference crystal (in our case, the ideal fcc lattice at zero temperature) within a sphere of radius r:

$$\Lambda(r)=N^{-1}\int_0^r |Z^d(r')-Z^c(r')|dr', \tag{3.3}$$

where

$$Z(r)=\int_0^r 4\pi r^2\rho(r')dr' \tag{3.4}$$

is the coordination number, i.e., the average number of neighbors of an atom within a distance r. If $r_{\max}$ is chosen large enough that the value of the integrated distribution function for the disordered structure, $Z^d(r_{\max})$, is approximately equal to that of the idealized structure, $Z^c(r_{\max})=N_{\max}$, then $\Lambda(r_{\max})$ can be used as a global disorder parameter.

As an illustration, we consider, corresponding to the simplest example of a disordered system, the case of crystalline nickel at 1400 K, i.e., quite close to its melting point ($T_m^{\mathrm{Ni}}=1726$ K); the corresponding function $Z^d(r)$ is shown in Fig. 2. We find that thermal disorder is significant already in the hot crystal, since in contrast to this, $Z^c(r)$ increases stepwise (i.e., discontinuously) at every new shell of neighbors in the reference, $T=0$, crystal. In the lower panel of Fig. 2, the quantity $|Z^c(r)-Z^d(r)|$ is displayed. The calculated value of Λ at this temperature is 0.049, in units of the fcc lattice constant. The corresponding values at 300 and 600 K are, respectively, 0.031 and 0.037.

B. Highly-disordered structures: General grain boundaries and the amorphous state

As mentioned in Sec. II, general high-angle grain boundaries are difficult to model and, therefore, an amorphous structure will be used to approximate the worse possible situation. In order to generate the amorphous structure, we use the technique of molecular dynamics (MD) to first melt a crystalline sample, then quench it to a disordered state.[33] The MD simulations were performed at constant pressure. The temperature was initially raised by rescaling the velocities, while the "Nosé thermostat" method[32] was used to control the temperature in the final stage of the runs.

It is known that pure nickel does not exist in stable amorphous form unless it is rapidly cooled from the melt on a very low-temperature substrate.[34] Following this logic, we generated an amorphous nickel structure by first taking a crystalline Ni structure to a temperature of 2000 K (which causes it to melt), equilibrating long enough that the system completely loses memory of its original crystalline state ($\Lambda=0.066$ in equilibrium), then cooling rapidly to 100 K and equilibrating again. In Fig. 3 we show the configuration-averaged pair distribution function for an amorphous nickel sample which contains 108 atoms. It should be noted that the volume of the amorphous nickel structure is, as expected, larger (by 3.6% at 100 K) than the corresponding crystalline sample. The calculated distribution function agrees well with experimentally measured pair distribution functions.[35] The calculated Λ of the amorphous structure is slightly smaller than that of the liquid state and equals 0.064.

C. Structure of special grain boundaries

Special grain boundaries with low Σ values have high symmetry and consequently only a small unit cell is needed to represent their structure, which will simplify the subsequent magnetic-moment calculations. The smallest unit cell for [100] twist grain boundaries is provided by the $\Sigma=5$ (36.9° twist) grain boundary. Here we investigate both the $\Sigma=5$ [100] and the [100] $\Sigma=13$ (22.6° twist), so as to analyze the influence of the twist angle on the local moments. The relaxed structure of these grain boundaries were obtained, again, using MD at a temperature of 100 K. Periodic boundary conditions were used to eliminate the surfaces.

The relaxed structure of the grain boundaries are shown in Fig. 4 and Fig. 5. The MD supercell contained 70 and 182 atoms for the $\Sigma=5$ and $\Sigma=13$ grain boundaries, respectively. This means that the spacing between periodic images of the grain boundaries is rather small (seven layers). This is

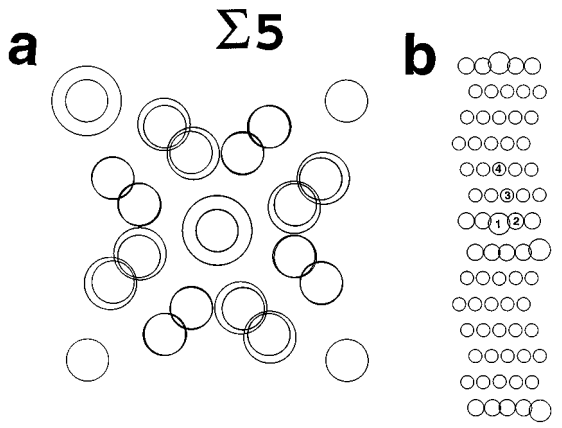

FIG. 4. The relaxed structure of the Σ5 grain boundary projected along (a) (001) and (b) (010). The large circles correspond to Ni(1) sites and the medium-sized ones to Ni(2). The sites in the second and subsequent layers from grain boundary are labeled Ni(3) and Ni(4), respectively.

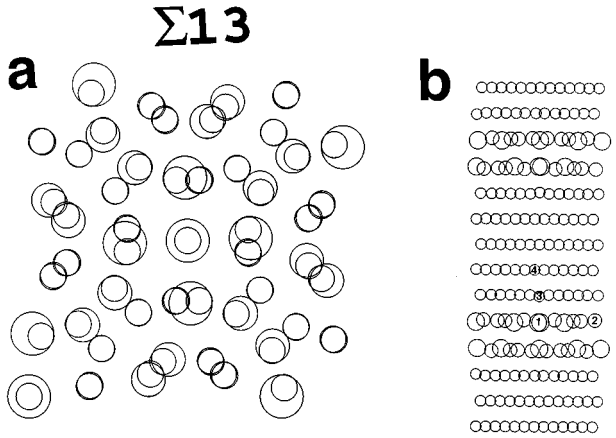

FIG. 5. Same as Fig. 4, but for the Σ13 grain boundary.

beneficial in reducing the computer time for the subsequent electronic-structure calculations. This, we have verified, has little effect on the local magnetic moments.

As can be seen in Figs. 4 and 5, there is a significant increase in the interlayer spacing near the grain boundary in the direction perpendicular to it. However, not all atoms in the layer which is closest to the grain boundary are shifted by the same distance. Some of them, represented by large circles in Fig. 4 and which we label Ni(1), are shifted less than the other ones in the layer, represented by intermediate circles, and which we label Ni(2). We note, in contrast, that shifts in the x and y directions are small for all sites. [For futher reference, we use the labels Ni(3) and Ni(4) for the atoms in the second and subsequent layers, respectively.]

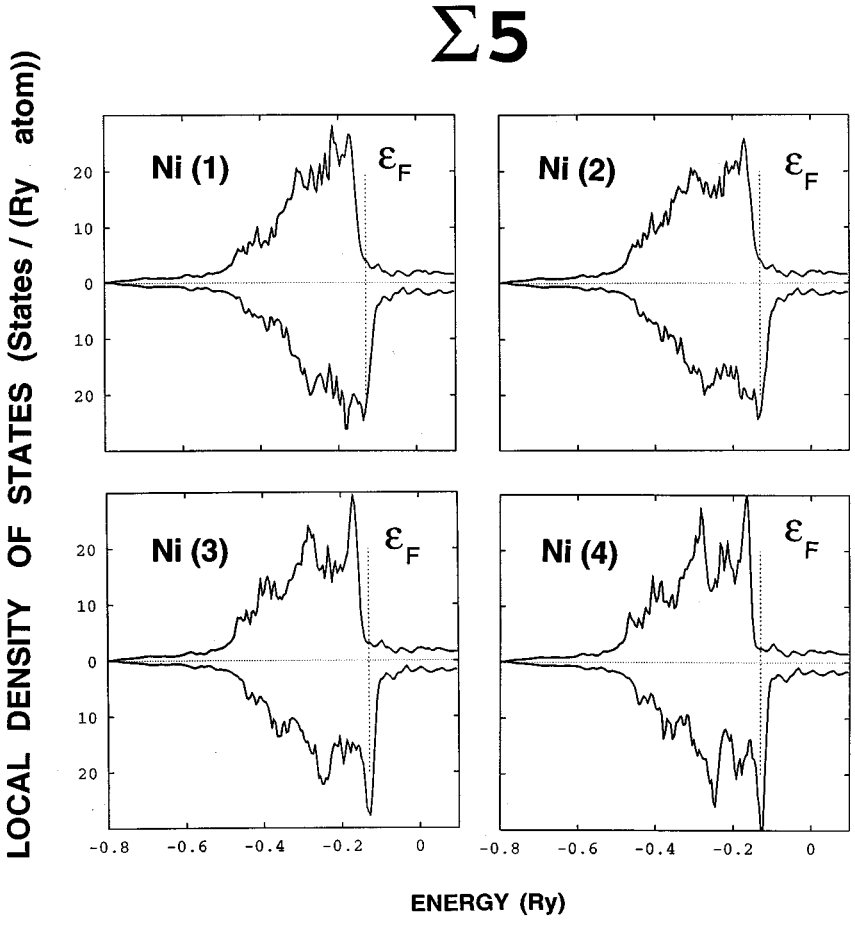

FIG. 6. Local density of states per atom for the various sites (as indicated; cf. Fig. 4) of the Σ5 grain boundary, for spin up and down electrons, respectively.

D. TB-LMTO-ASA calculations of the magnetic moments in special grain boundaries

The linear muffin-tin orbital (LMTO), atomic-sphere approximation (ASA) method, based on density-functional theory in the local density approximation, is known to be a good approximation for closely packed systems; it has been successfully used for rare earth and transition metals.[36–38] It has been shown[38] that this method leads to a simple first-principles tight-binding (TB) method. The advantage of the TB-LMTO-ASA method is that the transfer matrix factorizes with canonical structure constants which are energy independent. Therefore it needs to be calculated only once for a given crystal structure and a given set of potential parameters describing the atomic spheres. This feature of the method makes self-consistent calculations less time consuming and allows calculations for fairly complicated crystal structures to be performed.

In the present calculations, we employ a valence basis set of *s, p, d* electrons in the frozen-core approximation. An argonlike core is used for nickel atoms. The Von-Barth-Hedin local-spin-density approximation is used to describe the exchange-correlation energy.[39] In the self-consistency iterations, the spin-orbit coupling is neglected but all other quasirelativistic effects are included.

We have observed that it is very difficult to obtain self-consistency for individual sites. In order to resolve this difficulty, we have considered in the initial part of the calculation, all sites to be equivalent. After self-consistency of the *average* spin and charge density was reached, further iterations were performed, now allowing nonequivalent sites to be distinguished. The mixing parameter (for the charge and spin densities) was set, in the first iteration, to 1.0, and smaller values were used (0.005) in further iterations until self-consistency was obtained in the local moments (to within $0.001\mu_B$). (We will discuss below, in the case of the amorphous structure, the evolution of the local magnetic moment distribution between the first and the final iterations.)

TABLE I. Calculated local magnetic moments (in μ_B) (sites are labeled as indicated in the captions of Figs. 4 and 5), local average distances, $d(i)_Z$, and corresponding average absolute deviations, $\Delta d(i)_Z$, for the relaxed $\Sigma 5$ and $\Sigma 13$ grain boundaries.

Grain boundary	Site	Magnetic moment	$d(i)_Z$	$\Delta d(i)_Z$
$\Sigma = 5$	Ni(1)	0.48	1.039	0.039
	Ni(2)	0.53	1.051	0.072
	Ni(3)	0.55	1.004	0.012
	Ni(4)	0.57	1.001	0.006
$\Sigma = 13$	Ni(1)	0.56	1.031	0.027
	Ni(2)	0.57	1.034	0.058
	Ni(3)	0.58	1.004	0.015
	Ni(4)	0.58	1.002	0.007

The final calculations for the $\Sigma 5$ grain boundary were performed with a total of 64 **k** points. In Fig. 6, the local density of states for different sites is presented; the corresponding local moments are listed in Table I. The results are

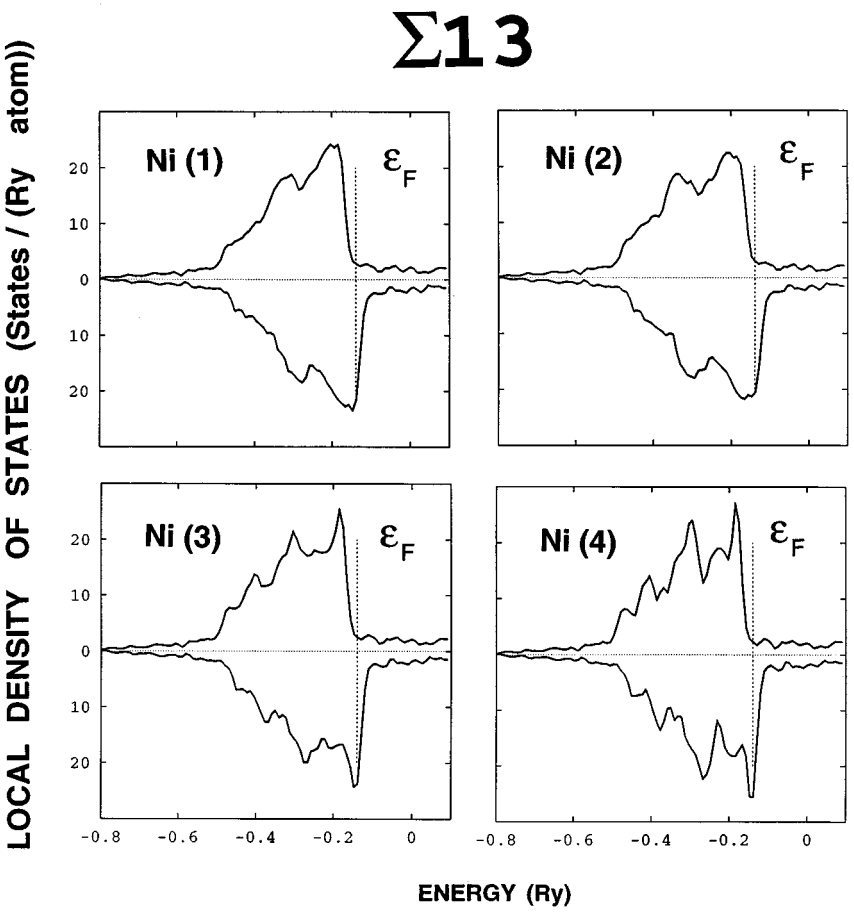

FIG. 7. Same as Fig. 6, but for the $\Sigma 13$ grain boundary.

rather similar to those for perfect fcc nickel atoms, except for the Ni(1) site—which lies closest to the grain boundary—where the sharp peak around the Fermi energy is lowered: the local moment on the Ni(1) site is reduced to $0.48\mu_B$. The local magnetic moment of the other sites, on the other hand, is closer to the value for the fcc structure, namely $0.58\mu_B$. Note, however, that even though the local moment on Ni(1) is reduced by about 20%, the total moment associated with this grain boundary is not significantly changed since Ni(1) sites constitute only a small portion of the total number of atoms.

For the $\Sigma 13$ grain boundary, we used only 30 **k** points, which is sufficient in view of the large size of the cell. For this grain boundary, the moment of Ni(1) atoms (i.e., near the grain boundary), $0.56\mu_B$, is changed less than corresponding sites in the $\Sigma 5$ case (Table I). We also give, in Table I, the $d(i)_Z$ and $\Delta d(i)_Z$ values for those sites. One conclusion that can be drawn from these data is that the amount of disorder and the value of the local magnetic moment are not unambiguously correlated. Evidently, $\Delta d(i)_Z$ tends to decrease when moving away from the grain boundary (i.e., order increases, as expected), and the magnetic moment increases correspondingly, tending to the ideal bulk value of 0.58. However, Ni(2) atoms have a larger magnetic moment than Ni(1), even though they are locally more disordered. This is also true of the relation between the magnetic moment and $d(i)_Z$. In Fig. 7 we present the corresponding density of states per atom for the $\Sigma 13$ grain boundary; it does not show much change from layer to layer except that due to the larger structural disorder at the grain boundary we observe ''smear out'' density of states for Ni(1) and Ni(2) . We see the characteristic peak at the Fermi energy which is present in the ideal fcc structure.

E. Amorphous nickel and general grain boundaries

We have also performed LMTO-ASA spin-polarized calculations for a highly-disordered (amorphous) state in order to investigate, as discussed earlier, if there could be a significant reduction of the magnetization at a general, random, grain boundary. An amorphous structure containing 108 atoms with periodic boundary conditions was thus constructed using the procedure described earlier. It has been shown[40,41] that modeling a liquid metal by a relatively small number of atoms in a periodically-replicated supercell yields reliable results for the electronic structure, in good agreement with photoemission, x-ray diffraction and Auger electron spectroscopy. Since the unit cell used here is rather large (in the sense of electronic-structure calculations), and in order to avoid artifacts resulting from the use of periodic boundary conditions, the self-consistency iterations were performed using only one **k** point, namely Γ. The final density of states shown in Fig. 8, however, was calculated with 27 **k** points. To eliminate the error of approximations when comparing the magnetic properties of crystalline and amorphous nickel, we concurrently performed calculations for a crystalline sample also containing 108 atoms and using the Γ point only for achieving the self-consistency. Similar to the amorphous state, we present in Fig. 9 the density of states calculated for 27 **k** points.

The calculated average moments per site are 0.61 and $0.50\mu_B$ for crystalline and amorphous nickel, respectively.

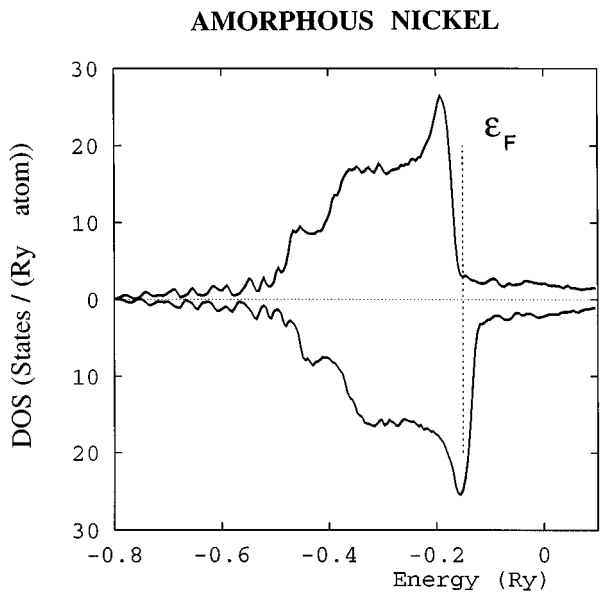

FIG. 8. Average density of states per site for amorphous nickel.

The local moment for crystalline nickel within this approximation is slightly larger than the value of $0.58\mu_B$ obtained using 2197 **k** points; the difference between the two values provides a measure of the accuracy of our calculations. In the case of amorphous nickel, we have reached self-consistency in spin and charge density for the average atom only. We present in Fig. 10 the distribution of local moments for 108 randomly chosen sites, after the average site has converged. As mentioned earlier, it is difficult to obtain self-consistency in charge and spin distribution when relaxing individual sites independently, as small oscillations persist even after several iterations; this problem was in fact also noted by other authors,[42] the local moments converging only to within $0.01\mu_B$. Figure 11 shows the distribution of local moments,

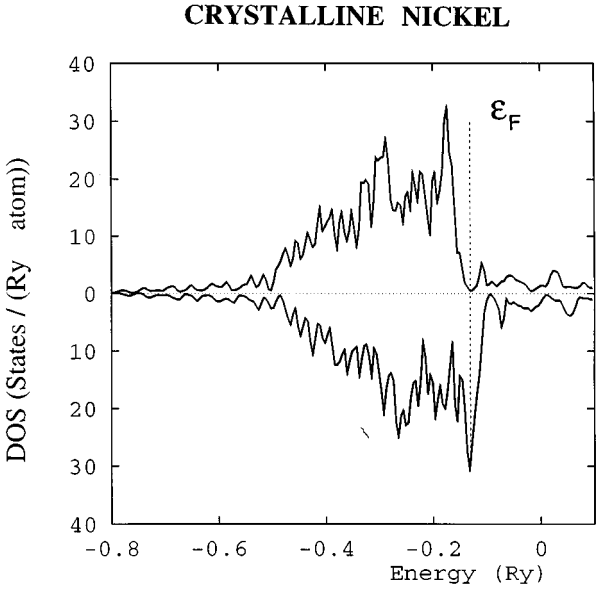

FIG. 9. Density of states for crystalline nickel.

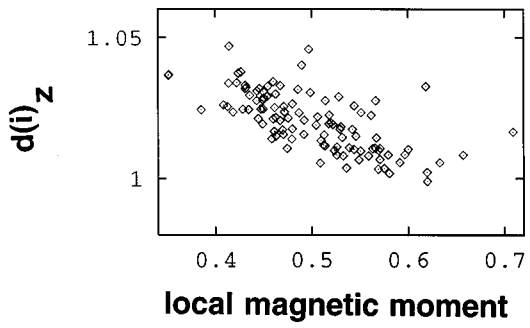

FIG. 10. Correlation between the local average nearest-neighbor distance, $d(i)_Z$, and the local magnetic moment calculated using one **k** point and a cluster of 108 atoms with pair distribution function shown in Fig. 3. Self-consistency was obtained for the average moment.

for the same 108 sites as above but after convergence of $0.001\mu_B$ for the local magnetic moments has been obtained. While the average moment does not change much in subsequent iterations, the distribution of local moments is narrowing around its average value, as can be seen by comparing Figs. 10 and 11: the standard deviation of the distribution is equal to $0.064\mu_B$ in the former case, and to $0.039\mu_B$ in the latter case, while the average moment is approximately constant at $0.50\mu_B$. Our findings explain why, in previous first-principles calculations where only average site density convergence was imposed,[22] a much wider distribution of local moments was found, i.e., local self-consistency[42] was not reached. It is of interest to note from both Figs. 10 and 11 that the average local moment has a tendency to increase when the average distance approaches that of the fcc crystal.

Our results for amorphous nickel are consistent with recent calculations for Co and Fe which predict little or no change in the magnetic moment when the structure changes from crystalline to amorphous.[20,42] On the other hand, fairly large changes in the saturation magnetization (up to 40%) were observed experimentally[34] when initially amorphous Ni films were crystallized by annealing. These results,[34] however, are difficult to interpret since the reduction in Curie temperature was only 15% and no absolute magnetization values were given. In addition the authors[34] did not consider

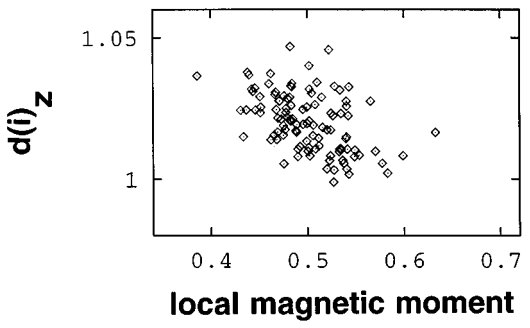

FIG. 11. Same as Fig. 10, but with the self-consistency obtained for 108 individual sites, and in an average way for the remaining sites, as discussed in the text.

in their interpretation other microstructural changes during annealing which may account for the increased saturation magnetization of their crystallized Ni. Such changes may include an increase in the effective surface area of the crystallized sample due to grain boundary grooving, island formation, spheroidization, etc., which may be expected during the annealing of thin polycrystalline films.

Our calculations demonstrate that the average magnetic moment is rather insensitive to the amount of structural disorder present, whether at a grain boundary interface or overall throughout the structure, and we conclude that this is true also of nanocrystalline materials. Even assuming that *all* grain boundaries in nanocrystalline nickel were of the amorphous kind discussed above which, we recall, is the worst possible case of a general grain boundary, the average magnetic moment would not be reduced by more than 15% from its crystalline counterpart; even smaller effects are expected for materials containing special and regular (nonamorphous) random grain boundaries. These results are fully consistent with the observation, in fully dense nanocrystalline nickel produced by electrodeposition[16] of a remarkable constancy of the saturation magnetization as a function of grain size, down to about 10 nm.

In order to assess the overall effect of grain boundaries on the saturation magnetization of nanocrystalline materials with even smaller grain size, it then becomes important to study two key parameters: first, the total interfacial volume fraction, which increases rapidly with decreasing grain size[2] and, second, the grain boundary character distribution in the material. The latter is of importance because, evidently, the average magnetic moment of the grain boundary component will be determined by the relative frequencies of occurence of different types of grain boundary structures.

Our results indicate, on the other hand, that for conventional polycrystalline materials (with grain sizes larger than 1 μm), increasing the relative number of special grain boundaries by interface control processing[24] is not likely to have a strong effect on the saturation magnetization. This is because the intercrystalline volume fraction (and therefore its contribution to the overall magnetization) in such conventional materials is negligible. However, the influence of the porosity on the magnetic properties is still an open question. In nanocrystalline materials prepared by compaction of nanocrystalline powders, the porosity is generally larger than in electroplated materials.[16] In pure Ni, this would lead to an effective increase of the distances between nickel atoms and the narrowing of the band in analogy to the magnetism on Ni surfaces,[43] for which an increase of the local moments of up to 20% has been reported. However, the opposite effect is observed experimentally, a significant decrease in the magnetization in gas-condensed nanocrystalline material containing high levels of porosity. One possibility is that in porous materials, the decrease in the magnetization saturation at room temperature (compared to low temperature values) is due to a reduction in the number of nearest neighbors at pore surfaces, leading to a concomitant reduction of the effective field and therefore a fast drop in the magnetization with temperature.[17] Further investigation of the magnetization saturation at low temperature for gas-condensed material would be very valuable to clear this point.

F. Influence of the foreign atoms on the magnetic properties of nanocrystalline nickel

Another possibility is that a large difference in the grain size dependence of the saturation magnetization between electroplated Ni and Ni produced by inert gas condensation and subsequent compaction is due to the presence of foreign atoms such as oxygen. In fact, Gong *et al.*,[12] Du *et al.*,[13] and Gangopadhyay *et al.*[11] have attributed the reduction of saturation magnetization (M_s) in their gas-condensed materials to the presence of an antiferromagnetic nickel oxide layer. We have recently studied the sensitivity of the magnetic moment to added impurities for the example of fully dense electroplated nanocrystalline nickel containing various amounts of phosphorus in solid solution.

Nickel is a band ferromagnet with magnetic moment contribution coming mostly from *d* electrons. According to our TB-LMTO-ASA calculations using a large (2197) number of **k** points in the Brillouin zone, the majority band is almost filled, the difference between majority and minority band filling being equal to 0.58 electrons. If we assume that two *s* electrons and one unpaired *p* electron of the outer shell of phosphorus would fill unoccupied states in the minority band of nickel to make it nonmagnetic (according to the rigid-band model) then we would expect that at a concentration of 16 at. % P, Ni-P becomes paramagnetic. Experimentally we have observed that the saturation magnetization of Ni-P gradually decreases with increasing phosphorus content.[44] The transition to paramagnetic behavior was observed at about 15% phosphorus.

On the other hand, the impurities of transition metals in nickel have enhanced moments and this might help to increase the saturation magnetization in nanocrystalline nickel.[45]

We conclude that electroplated pure nanocrystalline nickel has a larger saturation magnetization than gas condensed materials due to the presence of clean grain boundaries and the absence of the nickel oxide phase. Lower porosity is another factor which leads to larger magnetization per unit volume and, as a result, better quality magnetic material.

IV. CONCLUDING REMARKS

The influence of structural disorder on the magnetic properties of nanocrystalline nickel has been studied. Various grain-boundary configurations (the $\Sigma 13$ and $\Sigma 5$ special grain boundaries and the extreme case of an amorphous structure) were minimized using molecular-dynamics simulations. The electronic-structure calculations were performed within the framework of local-spin-density functional theory using the TB-LMTO-ASA approach. Our calculations reveal that the magnetic moment is rather insensitive to the amount of disorder present in the structure, varying by at most 20%. These results correlate extremely well with the recent observation in electroplated nickel by Aus *et al.*[16] that the magnetic moment depends very little on grain size, down to about 10 nm, i.e., is not critically determined by the amount of matter in the grain boundaries. Even in the limit where all the volume belongs to interfaces, in the worse possible case that the structure of these interfaces is fully disordered, the magnetic moment is reduced by only about 15%. This further suggests that the large variations observed in large-porosity, gas-condensed material[12,1,9] must be due to the presence of impurity atoms (such as oxygen) in the nanocrystalline matrix.

ACKNOWLEDGMENTS

The authors wish to acknowledge financial support from the Natural Sciences and Engineering Research Council of Canada, the Ontario Centre for Materials Research, and the ''Fonds pour la formation de chercheurs et l'aide à la recherche'' of the Province of Québec.

[1] H. Gleiter, Prog. Mater. Sci. **33**, 223 (1989).
[2] G. Palumbo, S.J. Thorpe, and K.T. Aust, Scr. Metall. **24**, 1347 (1990).
[3] E.C. Stoner, *Magnetism and Matter* (Methuen & Co. Ltd., London, 1934).
[4] A.E. Berkowitz and E. Kneller, *Magnetism and Metallurgy* (Academic Press, New York, 1969).
[5] K. Hono, A. Inoue, and T. Sakurai, Appl. Phys. Lett. **58**, 2180 (1991).
[6] K. Hono, K. Hiraga, Q. Wang, A. Inoue, and T. Sakurai, Acta Metall. Mater. **40**, 2137 (1992).
[7] G. Herzer, Mater. Sci. Eng. **A133**, 1 (1991).
[8] K. Suzuki, A. Makino, N. Kataoka, A. Inoue, and T. Masumoto, Mater. Trans. JIM **32**, 93 (1991).
[9] W. Wagner, A. Wiedenmann, W. Petry, A. Geibel, and H. Gleiter, J. Mater. Res. **6**, 2305 (1991).
[10] U. Admon, M.P. Dariel, E. Grunbaum, and J.C. Lodder, J. Appl. Phys. **62**, 1943 (1987).
[11] S. Gangopadhyay, G.C. Hadjipanayis, B. Dale, C.M. Sorensen, and K.J. Klabunde, Nanostr. Mater. **1**, 77 (1992).
[12] W. Gong, H. Li, Z. Zhao, and J. Chen, J. Appl. Phys. **69**, 5119 (1991).
[13] Y.W. Du, M.X. Xu, J. Wu, Y.B. Shi, H.X. Lu, and R.H. Xue, J. Appl. Phys. **70**, 5903 (1991).
[14] S.H. Liou and C.L. Chien, J. Appl. Phys. **63**, 4240 (1988).
[15] R.D. Shull and L.H. Bennett, Nanostr. Mater. **1**, 83 (1992).
[16] M.J. Aus, B. Szpunar, A. M. El Sherik, U. Erb, G. Palumbo, and K.T. Aust, Scr. Metall. **27**, 1639 (1992).
[17] U. Herr, J. Jing, R. Birringer, U. Gonser, and H. Gleiter, Appl. Phys. Lett. **50**, 472 (1987).
[18] H.E. Schaefer, in *Mechanical Properties and Deformation Behaviour of Materials Having Ultra-Fine Microstructures, Vol. 233 of NATO Advanced Study Institute, Series E: Applied Sciences*, edited by M.A. Nastasi (Kluwer, Dordrecht, The Netherlands, 1992).
[19] J. Richter, K. Handrich, and J. Schreiber, Phys. Status Solidi B **68**, K61 (1975).
[20] U. Krauss and U. Krey, J. Magn. Magn. Mater. **98**, L1 (1991).
[21] I. Turek and J. Hafner, Phys. Rev. **46**, 247 (1992).
[22] Y. N. Xu, Y. He, and W. Y. Ching, J. Appl. Phys. **69**, 5460 (1991).

[23] M. Liebs, K. Hummler, and M. Fähnle, Phys. Rev. B **51**, 8664 (1995).
[24] G. Palumbo and K.T. Aust, in *Materials Interfaces*, edited by D. Wolf and S. Yip (Chapman and Hall, London, 1992), p. 190.
[25] M.L. Kronberg and F.H. Wilson, Trans. AIME **185**, 501 (1949).
[26] S. Ranganathan, Acta Crystallogr. **21**, 197 (1966).
[27] B. Szpunar, U. Erb, K.T. Aust, G. Palumbo, and L.J. Lewis, in *Interface Control of Electrical, Chemical, and Mechanical Properties*, edited by S. P. Murarka, K. Rose, T. Ohmi, and T. Seidel, MRS Symposia Proceedings No. 318 (Materials Research Society, Pittsburgh, 1994), p. 477.
[28] L. Dagens, J. Phys. F **16**, 1373 (1986).
[29] For a review of the MD technique, see M.P. Allen and D.J. Tildesley, *Computer Simulation of Liquids* (Clarendon, Oxford, 1987).
[30] For a review, see M.S. Daw, S.M. Foiles, and M. I. Baskes, Mater. Sci. Rep. **9**, 251 (1993).
[31] S.M. Foiles, M.I. Baskes, and M.S. Daw, Phys. Rev. B **33**, 7983 (1986).
[32] S. Nosé, J. Chem. Phys. **81**, 511 (1984).
[33] For a review, see J.-L. Barrat and M.L. Klein, Annu. Rev. Phys. Chem. **42**, 23 (1991); Y. Hiwatari, H. Miyagawa, and T. Odagaki, Solid State Ionics **47**, 179 (1991).
[34] K. Tamura and H. Endo, Phys. Lett. **29A**, 52 (1969).
[35] G.S. Cargill, in *Solid State Physics: Advances in Research and Aplications*, edited by H. Ehrenreich, F. Seitz, and D. Turnbull (Academic, New York, 1975), Vol. 30, p. 227.
[36] H.L. Skriver, *The LMTO Method* (Springer-Verlag, New York, 1984).
[37] O.K. Andersen, O. Jepsen, and D. Glötzel, in *Highlights of Condensed Matter Theory*, Proceedings of the International School of Physics ''Enrico Fermi,'' course 89, Varenna, 1983, edited by F. Bassani *et al.* (Elsevier, Amsterdam, 1985).
[38] O.K. Andersen, O. Jepsen, and M. Sob, in *Electronic Band Structure and its Applications*, edited by M. Yussouff (Springer-Verlag, Berlin, 1986), p. 440.
[39] V. von Barth and L. Hedin, J. Phys. C **5**, 1629 (1972).
[40] S.K. Bose, S.S. Jaswal, O.K. Andersen, and J. Hafner, Phys. Rev. B **37**, 9955 (1988).
[41] W. Jank and J. Hafner, Phys. Rev. B **41**, 1497 (1990).
[42] I. Turek, Ch. Becker, and J. Hafner, J. Phys. C **4**, 7257 (1992).
[43] E. Wimmer, H. Krakauer, and A.J. Freeman, Adv. Electron. Electron. Phys. **65**, 357 (1985).
[44] M.J. Aus, B. Szpunar, B. Judd, A.M. El Sherik, U. Erb, G. Palumbo, and K.T. Aust (unpublished).
[45] B. Szpunar and U. Erb (unpublished).